

## Trajectory displacement in a multi beam scanning electron microscope

Stopka, Jan; Zuidema, Wilco; Kruit, Pieter

**DOI**

[10.1016/j.ultramic.2021.113223](https://doi.org/10.1016/j.ultramic.2021.113223)

**Publication date**

2021

**Document Version**

Final published version

**Published in**

Ultramicroscopy

**Citation (APA)**

Stopka, J., Zuidema, W., & Kruit, P. (2021). Trajectory displacement in a multi beam scanning electron microscope. *Ultramicroscopy*, 223, Article 113223. <https://doi.org/10.1016/j.ultramic.2021.113223>

**Important note**

To cite this publication, please use the final published version (if applicable). Please check the document version above.

**Copyright**

Other than for strictly personal use, it is not permitted to download, forward or distribute the text or part of it, without the consent of the author(s) and/or copyright holder(s), unless the work is under an open content license such as Creative Commons.

**Takedown policy**

Please contact us and provide details if you believe this document breaches copyrights. We will remove access to the work immediately and investigate your claim.



# Trajectory displacement in a multi beam scanning electron microscope

Jan Stopka<sup>a,\*</sup>, Wilco Zuidema<sup>b</sup>, Pieter Kruit<sup>b</sup>

<sup>a</sup> Institute of Scientific Instruments, Czech Academy of Science, Královopolská 147 Brno, 612 64, Czech Republic

<sup>b</sup> Dept. Imaging Physics, Delft University of Technology, Lorentzweg 1, Delft, 2628CJ, The Netherlands

## ARTICLE INFO

### Keywords:

Trajectory displacement  
Multi-beam electron microscope  
Coulomb interactions  
Slice method  
Electron optics

## ABSTRACT

The analytical theory of statistical Coulomb interactions allows to determine the trajectory displacement in a single rotationally symmetrical beam with well-behaved spatial and angular particle distributions. This can be used to estimate the trajectory displacement in a multi-beam system using the so called fully-filled segment approximation. This approach predicts full compensation of trajectory displacement for a specific setup of the system. We show that this prediction is not consistent with Monte Carlo simulations and we develop a new approach to the calculation, showing that two independent trajectory displacement contributions are present in a multi-beam system. We support this calculation with Monte Carlo simulations as well as with experimental data from a multi-beam system.

## 1. Introduction

An important characteristic of a probe forming instrument such as a scanning electron microscope (SEM) or electron lithography machine is the probe size which in turn determines the achievable resolution of the system. The probe size is given by a combination of a variety of factors such as the magnification of the source size, geometrical aberrations, chromatic aberration and diffraction [2]. In addition to these effects, the beam is also affected by stochastic interactions between the electrons in the beam. This effect can be divided into longitudinal and transverse components. The longitudinal component is called Boersch effect and it causes broadening of the energy distribution and thus increases the spot size via chromatic aberration. In this article we are interested in the transverse component which directly changes the trajectory of electrons and therefore it is called trajectory displacement. It manifests as an apparent enlargement of the source size which corresponds to effective reduction of the source brightness.

There are several approaches to estimating the trajectory displacement in an electron beam, but they can be roughly categorized into three groups: Monte Carlo simulation, numerical calculation and analytical formulas. Each approach has its own advantages and disadvantages. Monte Carlo simulation can provide the closest approximation to a real system because equations of motion are solved directly for a particle set, which requires very few assumptions about the system. On the other hand Monte Carlo simulation can be very time consuming as

tracing of large numbers of interacting particles is a computationally challenging task. Moreover, the results of such a simulation are quantities and parameters (such as energy and position) for the simulated particle set. These can be used to calculate the trajectory displacement for a particular setting of the system, but it provides limited insight into trends and dependencies of the trajectory displacement on the various parameters of the system such as beam current or energy.

The numerical calculation covers a variety of methods to determine the trajectory displacement ranging from quite general integrals based on distribution of particle positions and velocities through complex calculations using Markov chains [3] to very specific calculations such as the slice method which is only valid in certain regimes of operation. A large part of this category was developed by Jansen in his doctoral thesis [4] and is based on the so-called extended two-particle approximation. This model assumes that the individual scattering events a certain particle experiences along its trajectory are uncorrelated. This is a reasonable assumption in the case of electron microscopy.

The extended two-particle approximation of statistical Coulomb interactions as presented by Jansen [4] starts by describing the trajectory displacement in a beam with general spatial and angular distributions. However, the general description can only give results in terms of a set of integral expressions which give a little insight into the dependence of the displacement on parameters of the system such as beam energy, current etc. For a few special cases it is possible to evaluate the integrals and obtain an analytical expression for the trajectory displacement.

\* Corresponding author.

E-mail addresses: [jstopka@isibrno.cz](mailto:jstopka@isibrno.cz) (J. Stopka), [p.kruit@tudelft.nl](mailto:p.kruit@tudelft.nl) (P. Kruit).

<sup>1</sup> For example a 1 keV beam of 100 nA current and radius of 1 mm is a typical Holtzmark regime representative and 1 keV with 1 nA and 10 μm radius is in pencil-beam regime. The Gaussian regime can only be relevant when angular current density divided by energy is comparable or more than about 0.005 Asrad<sup>-1</sup> eV<sup>-1</sup> [1] which usually never occurs in scanning electron microscope.

These cases define the various regimes of Coulomb interactions in the beam. The Coulomb interactions in an electron microscope are usually dominated by weak collisions [5] and therefore the most important regimes for a beam in an electron microscope are pencil-beam regime that describes a beam of particles with longitudinal separation much larger than their lateral distance and Holtzmark regime which corresponds to the opposite — a beam of particles where direction to a particle's closest neighbors is unrelated to the beam orientation. We only consider these two regimes and assume the contribution from the Gaussian regime (several collisions per electron) is negligible.<sup>1</sup> We also only consider Coulomb interactions accumulated along the electron column and we incorporate the interactions in the vicinity of the electron source into virtual source size and energy spread [6].

The formulae for trajectory displacement in various regimes are derived with the assumption of a field-free region with a cylindrically symmetrical beam (with uniform or Gaussian spatial and angular distribution). We are interested in the behavior of trajectory displacement in a multi-beam scanning electron microscope (MBSEM) and the situation in a MBSEM is more complicated. The system is not rotationally symmetrical and the spatial and angular distribution cannot be described by a simple function such as a uniform cylinder or a Gaussian. Evaluating the integrals analytically is not feasible for such distributions. Although numerical calculation of the trajectory displacement in a multi-beam is still possible, it would provide only a limited insight into the dependence of the trajectory displacement on various parameters of the system. On the other hand, an appropriate approximate description of the multi-beam distributions can lead to fully analytical expressions.

## 2. Beam geometry in a multi-beam system

A multi-beam scanning electron microscope is a probe forming electron microscope that utilizes an array of beamlets simultaneously focused onto the specimen to form an array of spots. Each of these spots generates its own signal which is then processed from all the spots simultaneously. The main advantage of a multi-beam SEM over a conventional SEM is the throughput increase provided by probing multiple sample locations in parallel.

Several concepts to generate multiple electron beams in an electron microscope exist [7], but over time one particular design became the most common approach. This design utilizes a single electron source (such as Schottky emitter) which illuminates an array of apertures. This array is on a different potential from nearby electrodes and thus each aperture acts as an individual electrostatic lens. If the aperture lenses are strong enough, an array of images of the source can form below the aperture lens array. This can then be imaged using a conventional SEM column onto the sample to create a focused array of spots. More about the optics of a multi-beam is covered elsewhere such as in [8–13].

With such multi-beam geometry, there are a few places of interest that we will refer to further on in this article. A plane where all beamlets are focused is called a beamlet cross-over plane or simply a beamlet cross-over. Between any two such planes there is always another plane where all beamlets meet (under paraxial approximation). We call this plane the common cross-over plane or just a common cross-over. To minimize distortion of the pattern and probes due to lens aberrations, it is useful to set the system such that inside each lens there is either the array of focused spots or the common cross-over where all beamlets meet on the axis [13]. This is schematically depicted in Fig. 1.

## 3. Slice method in a multi-beam SEM

The analytical formulae for trajectory displacement derived by Jansen are valid for a single electron beam with radially symmetrical spatial and angular distributions. If the number of beamlets of the MBSEM is sufficiently large, we can approximate the multi-beam with a large single electron beam [14]. This approximation allows to express the trajectory displacement with analytical formula as a

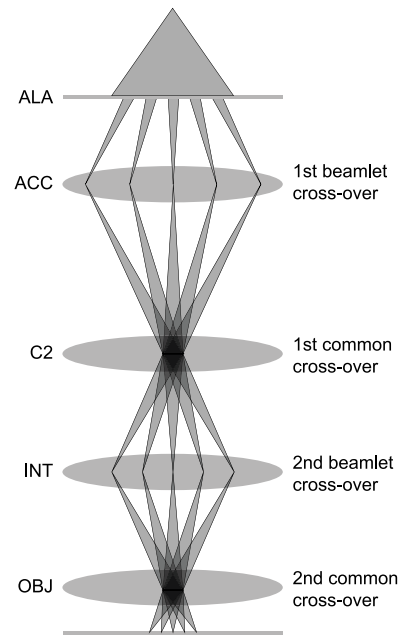


Fig. 1. Schematic drawing of a multi-beam scanning electron microscope optical column. From top to bottom there is a single electron source illuminating an aperture lens array (ALA), which forms an array of beamlets. The beamlets form an array of focused spots (1st beamlet cross-over) in the accelerator lens (ACC) which is then imaged with a conventional imaging system (C2, INT and OBJ lenses) onto the sample. To minimize distortion of the pattern due to lens aberrations, it is useful to set the system such that inside each lens there is either the array of focused spots (beamlet cross-over) or the common cross-over where all beamlets meet on the axis [13].

function of experimental variables such as beam current, energy and beam geometry.

The following theory describes the trajectory displacement in the central beamlet of a multi-beam system. It is possible to use the formulae for a corner beamlet as well with a few parameter substitutions and to estimate the trajectory displacement in all other beamlets using interpolation between the two cases as they usually do not differ a lot. We refer the reader to [14] for a detailed explanation of these transformations.

For beams that are not clearly in one of two regimes, Jansen proposes to add the separately calculated displacements using a power sum rule. It is however not advisable to use the power sum rule for a beam segment that has one end in the Holtzmark regime and the other end in the Pencil beam regime. The reason is that the displacement in the Holtzmark calculation will be dominated by the beam part that is actually in the pencil beam regime and vice-versa [15]. The result is an overestimation of the trajectory displacement.

One way around this problem is to use the slice method and use the power sum to combine differential trajectory displacement contributions which are then numerically integrated along the beam trajectory. In that case, as shown in [15], we can express the full-width 50% of the total trajectory displacement in the image plane as

$$FW_{50} = -\frac{C_\alpha}{m\sqrt{V(z_i)}} \int_{z_0}^{z_1} s_c(z) u_\alpha(z) \frac{I^2}{V^{3/2}(z)} (\chi^{8/7}(z) + \chi^{-6/7}(z))^{-7/6} dz, \quad (1)$$

where  $C_\alpha = 1.02905 \cdot 10^{18} \text{ V}^2 \text{ A}^{-2} \text{ m}^{-1}$ ,  $m$  is angular magnification of the system,  $V(z)$  is the beam energy along the axis,<sup>2</sup>  $u_\alpha$  is the axial

<sup>2</sup> We could take relativistic effects into account by replacing  $V$  with the relativistic beam potential  $V^* = V(1 + eV/2m_0c^2)$ . Usually though, the trajectory displacement in an electron beam is negligible for relativistic beam energies.

paraxial ray trajectory,  $I$  is the beam current,  $s_c(z)$  is either 1 or  $-1$  and changes sign with every common cross-over and finally  $\chi$  is the pencil-beam factor defined in [15] as

$$\chi(z) = C_\chi \frac{Ir(z)}{V(z)^{1/2}}$$

with  $C_\chi = 2.51979 \cdot 10^{13} \text{ V}^{1/2} \text{ A}^{-1} \text{ m}^{-1}$  and  $r(z)$  the beam radius.<sup>3</sup> This factor defines whether the beam is in a pencil-beam regime ( $\chi \ll 1$ ) or in Holtzmark regime ( $\chi \gg 1$ ). The pencil-beam factor can be roughly interpreted as the number of particles in a cubic volume of similar dimensions to the diameter of the beam. Since the radius of the beam varies a lot along the trajectory, it is not unusual for the beam to transition between the two regimes.

Another approach to deal with the transition between the regimes is to use analytical formula for the funnel regime. This is an expression which converges to Holtzmark and pencil-beam expressions in the corresponding limiting cases, but interpolates well in the case a transition between the two regimes occurs. Since the formula is rather complicated, we omit it here and instead refer the reader to [15], where both the (generalized) slice method and the funnel regime formula are described in detail.

### 3.1. Compensation of trajectory displacement in MBSEM

Note the product  $s_c(z)u_\alpha(z)$  in the slice method integral (1). These parameters are the only factors which can change sign along the trajectory. In standard single beam probe forming systems, the beam crossovers coincide with the zeros of the ray trajectory and therefore the sign of  $s_c$  is equal to the sign of  $u_\alpha$  and the contribution to the trajectory displacement is positive throughout the whole trajectory. However, in the case of a MBSEM the  $s_c$  changes sign at common crossover(s) and  $u_\alpha$  corresponds to axial paraxial ray trajectory of any particular beamlet and thus changes sign at the plane of beamlet crossovers which is different from the common crossover position.

Consequently, there are parts of the multi-beam path where the trajectory displacement is in fact decreasing. This can be explained using the fact that the displacements in subsequent slices are highly correlated (a property of weak collisions). Thus the displacement experienced by a test particle traveling along the optical axis is in opposite direction after the particle passes the common crossover (see Fig. 3 top).

A notable case is a segment of a multi-beam between two planes of beamlet crossovers. Such a segment has a common crossover and a lens. If both the common crossover and the lens are positioned in the middle of such segment, the function  $u_\alpha$  is symmetric and  $s_c$  anti-symmetric with respect to the common crossover. Assuming the beam energy is constant in the segment this means the integral (1) vanishes and the trajectory displacement in such a segment would be zero.

This situation provides an ideal test case for comparison of the theoretical calculation to a Monte Carlo simulation.

### 3.2. Comparison with Monte Carlo simulation

We will compare the slice method calculation to a Monte Carlo simulation using the GPT software [16]. This software allows us to trace individual electrons through the system by numerical solution of equations of motion. The trajectory displacement can be calculated by comparing calculation with and without the Coulomb interactions taken into account. When a sufficient number of particles is traced, the distribution of the trajectory displacement can be estimated by direct comparison of particle positions in a particular plane along the axis in

<sup>3</sup> The pencil-beam factor is also defined in earlier works by Jansen [1,4,5], but there is a slight difference in the constant  $C_\chi$ . We used such value that there are no additional constants in the sum in Eq. (1).

the two cases (with and without Coulomb interactions). Various metrics of this distribution such as  $FW50$  can then be calculated. We chose parameters of the system to represent a typical situation in a MBSEM such as the one described in [11,13].

The situation comprises of a square array of  $13 \times 13$  point like sources of particles at plane  $z = 0$ . Electron beamlets from these sources are directed towards a common crossover at  $z = L/2 = 0.15 \text{ m}$ . There is a magnetic field of a lens located at the position of the common cross-over. This lens images the array of points at  $z = 0$  into image plane at  $z = L = 0.3 \text{ m}$ , thus the magnification of the lens is equal to negative one. The pitch of the multi-beam pattern in the object plane is  $80 \mu\text{m}$ . The particle energy is  $10 \text{ keV}$ . Finally, the size of the common-crossover is chosen such that the angular current density of a beamlet is  $0.3 \text{ mA/srad}$ . The calculation and simulation is done for a series of beamlet currents. In the case of the smallest current, the multi-beam is in pencil-beam regime across the whole segment. On the other hand for the largest current in the series, the multi-beam is in Holtzmark regime in the whole segment. For the intermediate values, there is a transition between the regimes.

For better understanding of the trajectory displacement, we have simulated and calculated the trajectory displacement (in the image plane) as a cumulative function of the position in the segment. In other words, we calculated the trajectory displacement as a function of the upper bound  $z_1$  of the integral (1). This is a good way to visualize the accumulation of the trajectory displacement in the first half of the segment and consequent compensation in the second half. Both the calculation and the simulation correspond to the central beamlet. The comparison is shown in Fig. 2.

In the figure we can see that in the first half of the segment, the slice method predicts a correct trend. However, after passing through the common crossover, the slice method predicts full compensation of the trajectory displacement, but the Monte Carlo simulation shows that the trajectory displacement is not compensated and for larger currents even continues to rise.

This is a large inconsistency between the theoretical prediction and a Monte Carlo simulation that calls for a further investigation.

## 4. In-beamlet interactions

The discrepancy is caused by the unjustified assumption of the slice method that the field particle maintains its orientation with respect to the test particle's trajectory.<sup>4</sup> This is the case for a beam with a narrow crossover. However, in the case of the multi-beam, the common crossover dimensions are not negligible and therefore a particle's position in the common cross-over and its vicinity is almost independent of the position far from the common cross-over (i.e. independent of which beamlet it is in). This means the displacement that a certain particle experiences in the region of the common cross-over is independent of the displacement from the regions outside of the common cross-over. The situation is depicted in Fig. 3.

As a result it is necessary to calculate the common cross-over region separately and then add it to the rest with an appropriate power sum rule (corresponding to the distribution of the displacements). What remains is how to divide the slices into common cross-over region and the rest.

<sup>4</sup> The test particle is a particle traveling along the optical axis. We are interested in the trajectory displacement of the test particle(s). The field particle on the other hand is any other particle that influences the test particle's trajectory.

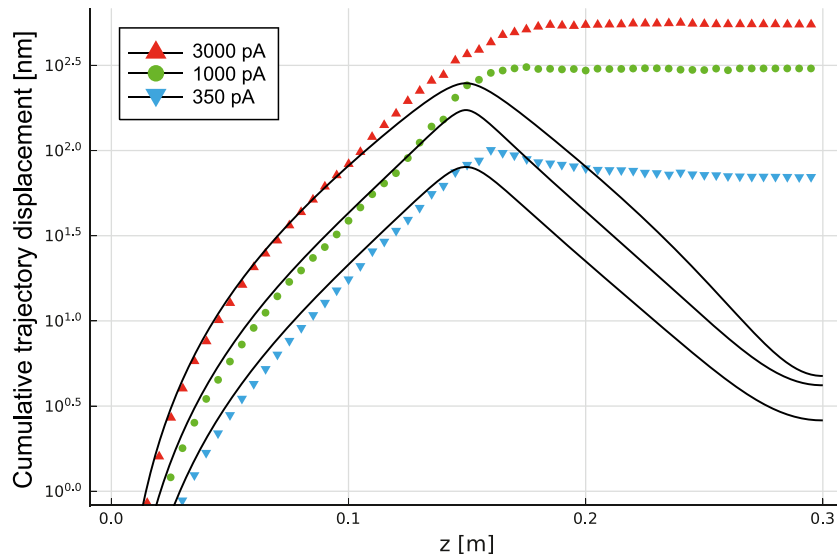


Fig. 2. The trajectory displacement as accumulated across a multi-beam segment with a lens in the common cross-over for various beamlet currents. The solid line shows the result of the slice method calculation using (1) and the dots show results of the Monte Carlo simulation.

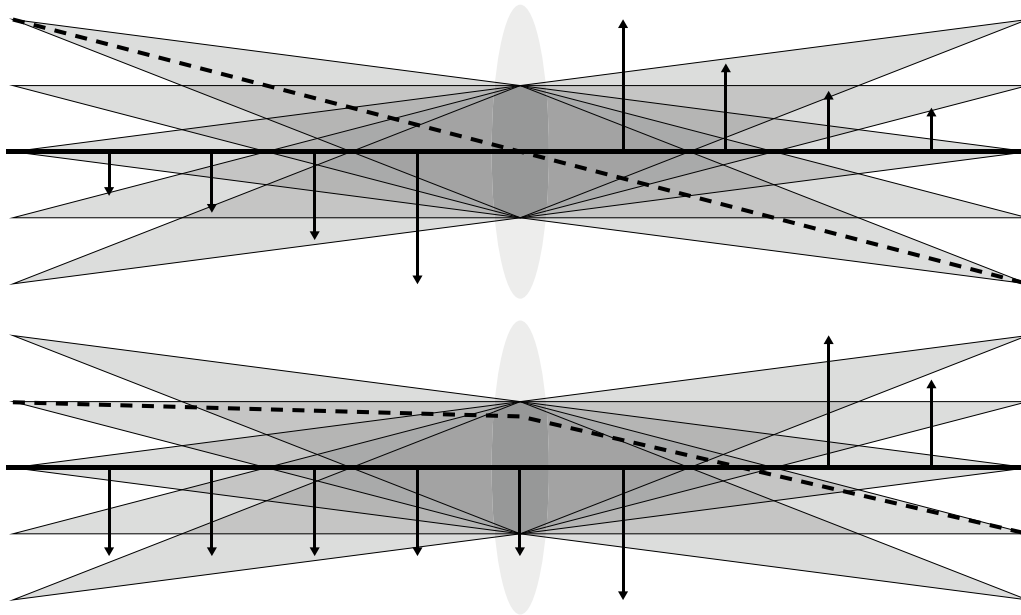


Fig. 3. The force exerted on a test particle (solid line) by a field particle (dashed line) for two distinct field particles in a multi-beam segment with a lens in a common cross-over. Top: The field particle is from a different beamlet, but meets the test particle on axis in the common cross-over. The displacement above the common cross-over is compensated by displacement below the common cross-over. This situation corresponds to the traditional expression for trajectory displacement described by Eq. (1). Bottom: The field particle is significantly distant from the test particle in the common cross-over. The displacement accumulated near the common cross-over is not compensated. Moreover, the field particle can be displaced in a direction perpendicular to the plane of the drawing, which also prevents the displacement from the common cross-over region to be compensated.

#### 4.1. Two-component model of the interactions

We propose a model that takes the correlation in mutual particle position along the slices into account. The direction (and thus also the displacement) of the field particle with respect to the test particle near the beamlet cross-overs is independent of the direction between the two particles at the common cross-over. Therefore, we can model the two displacements as mutually perpendicular dimensions; let us call them  $\vec{a}$  and  $\vec{b}$  respectively.<sup>5</sup> The displacement in a slice located at the

beamlet cross-overs is in direction  $\vec{a}$  and the displacement in a slice at the common cross-over is in direction  $\vec{b}$ .

The last step is to assign some orientation in this new abstract 2D displacement space to all the other slices. That can be done by interpolating:

$$\vec{v}(z) = \frac{r_f(z)\vec{a} + r_a(z)\vec{b}}{\sqrt{r_f(z)^2 + r_a(z)^2}}, \quad (2)$$

where  $r_f(z)$  is the beamlet central trajectory of an average beamlet and  $r_a(z)$  is the axial ray trajectory of an average particle of the central beamlet. The trajectory  $r_f$  can be interpreted as the mean multi-beam radius and  $r_a$  as the mean beamlet radius. By taking those radii signed (i.e.  $r_f$  changing sign in the common cross-over and  $r_a$  changing sign in the beamlet cross-over) the two components correspond to the

<sup>5</sup> It is important not to confuse the abstract displacement dimensions  $\vec{a}$  and  $\vec{b}$  with real coordinate dimensions  $\vec{x}$  and  $\vec{y}$ . Both  $\vec{a}$  and  $\vec{b}$  displacements can still have any direction in the real space with the mean direction equal to zero.

correlation of mutual particle transverse position at  $z$  with their mutual transverse position in the plane of beamlet cross-overs and the common cross-over respectively. In (1) the correlation is represented by the sign function  $s_c(z)$  but it is limited either to full correlation ( $s_c = 1$ ) or full anti-correlation ( $s_c = -1$ ). The natural next step is to take the changing correlation into account and replace this sign function  $s_c$  in the integral with the slice displacement direction  $\vec{v}(z)$  defined by (2).

With that we can finally express the two components of the trajectory displacement as

$$FW_{50,a} = -\frac{C_\alpha}{m\sqrt{V(z_i)}} \int_{z_0}^{z_1} \frac{r_r(z)}{\sqrt{r_r(z)^2 + r_\alpha(z)^2}} u_\alpha(z) \times \frac{I^2}{V^{3/2}(z)} (\chi^{8/7}(z) + \chi^{-6/7}(z))^{-7/6} dz, \quad (3)$$

$$FW_{50,b} = -\frac{C_\alpha}{m\sqrt{V(z_i)}} \int_{z_0}^{z_1} \frac{r_\alpha(z)}{\sqrt{r_r(z)^2 + r_\alpha(z)^2}} u_\alpha(z) \times \frac{I^2}{V^{3/2}(z)} (\chi^{8/7}(z) + \chi^{-6/7}(z))^{-7/6} dz. \quad (4)$$

The two expressions differ only in the factor  $r_r(z)$  or  $r_\alpha(z)$  in the integrand. We can see that the sign of the two integrands depends only on the sign of  $r_r(z)u_\alpha(z)$  and  $r_\alpha(z)u_\alpha(z)$  respectively. The first product can be positive or negative depending on the sign of the factors, but the second product is always non-negative because  $r_\alpha(z)$  is a positive multiple of  $u_\alpha(z)$ . Consequentially, the  $a$  component of the trajectory displacement can be fully compensated with a suitable design of optical trajectory, while the  $b$  component always gives positive contribution to the total trajectory displacement.

The total trajectory displacement distribution is a convolution of the displacement distribution for  $\vec{a}$  and  $\vec{b}$  directions. Its  $FW_{50}$  can be approximated with a power sum rule as

$$FW_{50} = \left( FW_{50,a}^\gamma + FW_{50,b}^\gamma \right)^{1/\gamma}. \quad (5)$$

The power  $\gamma$  depends on the regime. We have  $\gamma = 1/3$  for pencil-beam regime and  $\gamma = 3/2$  for Holtzmark regime [4]. In the case a transition between the regimes occurs, some effective power in between the two values should be chosen.

## 4.2. Comparison of the new model with Monte Carlo simulation

We can now compare the results calculated using the new model with the Monte Carlo simulation from Section 3. The comparison is depicted in Fig. 4. We can see that the new model of two mutually uncorrelated contributions to the trajectory displacement agrees with the simulation very well.

## 5. Experimental verification

Comparing a theoretical model to a Monte Carlo simulation is useful, but not a full validation of the theory. After all, the real situation can present unforeseen effects excluded both from the theory and from the simulation. In the following, we try to verify the theoretical prediction with an experimental measurement.

### 5.1. Description of the experiment

We use a modified FEI NovaNano SEM with a multi-beam source (196 beamlets). This MBSEM has a parallel transmission detection system [17]. A thin sample is put directly on a YAG screen. An array of electron beams therefore creates an array of light sources which are then imaged onto a light detector. In our setup we used a single pixel detector to observe just one of the beamlets. Scanning with the multi-beam pattern moves one of the beams across the sample which varies the light intensity captured by the single pixel light detector thus forming an image. By detecting only the light coming from one of the beamlets we are able to form an image with a single beamlet.

In the standard mode of operation, the multi-beam source creates an array of beamlet cross-overs inside the source module which is then demagnified with the objective lens onto the sample. However, this also demagnifies the trajectory displacement accumulated along the trajectory. After such demagnification the trajectory displacement is comparable or smaller than aberrations of the system. The only information we get is provided by imaging a sample with the probe. Spot size and even its distribution function can be deduced from these images, but the trajectory displacement cannot be seen separately from other effect influencing the spot size. Therefore, demagnifying the trajectory displacement makes it hard to separate the trajectory displacement from the final spot size.

Fortunately, there is a so called intermediate lens located in the middle of the column. We can use this lens as a final lens to image the array of beamlet cross-overs onto the sample with magnification close to unity and thus reduce the demagnification of the trajectory displacement and decreasing the effect of lens aberrations. This is schematically shown in Fig. 5.

With such a configuration, the spot size on the sample is in the order of hundreds of nanometers. This limits the sample choice. We have used a sample with a pattern of stripes with a pitch of  $1 \mu\text{m}$ . The width of the stripes is  $0.65 \mu\text{m}$ . Such sample has the advantage that we do not need to have perfectly focused and stigmated spot, because in case of a small defocus, we can use the stigmator to create a line focus parallel to the stripes, therefore achieving the same image quality as if the spot was perfectly stigmatic and in focus.

A typical image of the sample created with one of the central beamlets is shown in Fig. 5. Darker intensity in corners of the image is caused by the light spot missing the detector.

This image can then be automatically processed to calculate the  $FW_{50}$  of the spot. A conventional approach to measure the spot size would be to use deconvolution. The acquired image is theoretically formed as a convolution of a sharp image of the sample and the distribution function of the probe. However, in our case the image is also influenced by limitation of the single pixel light detector which causes the intensity to drop towards the edges of the image. Due to this limitation, the deconvolution approach was unsuccessful and another method had to be chosen.

The spot size is determined by calculating the ratio between maximum and minimum intensity in the central part of the image. This ratio depends on the spot size, its distribution function, sample geometry and the ratio between the intensity of a dark and light stripe for perfect resolution image.

Let us assume that a point-like probe positioned inside the lighter stripe corresponds to relative signal intensity  $A$  and the probe positioned inside the darker stripe corresponds to intensity  $B$ . Next, let us denote the width of the light stripe as  $a$  and the width of the dark stripe as  $b$ . Finally, let us assume the sample is illuminated only by a single rotationally symmetrical electron probe with knife edge size of  $E_{25,75} = 2R$  and scaled linear cumulative distribution function  $F$ . The scaled linear cumulative distribution function can be calculated from the probe distribution function  $\rho(x, y)$  as

$$F(r/R) \propto \int_0^r dx \int_{-\infty}^{\infty} dy \rho(x, y) \quad (6)$$

We assume the scale of the function  $F$  to be such, that  $F(0) = 0$ ,  $F(1) = 0.5$  and  $F(\infty) = 1$ .

The intensity of the light and the dark stripes imaged with a probe with distribution  $F$  is then given respectively as

$$I_1 = B + (A - B) \left\{ F\left(\frac{a}{2R}\right) + \sum_{i=1}^{\infty} \left[ F\left(\frac{a/2 + i \cdot (a+b)}{R}\right) - F\left(\frac{-a/2 + i \cdot (a+b)}{R}\right) \right] \right\} = B + (A - B) S_1(R), \quad (7)$$

$$I_2 = A - (A - B) \left\{ F\left(\frac{b}{2R}\right) + \sum_{i=1}^{\infty} \left[ F\left(\frac{b/2 + i \cdot (a+b)}{R}\right) \right] \right\}$$

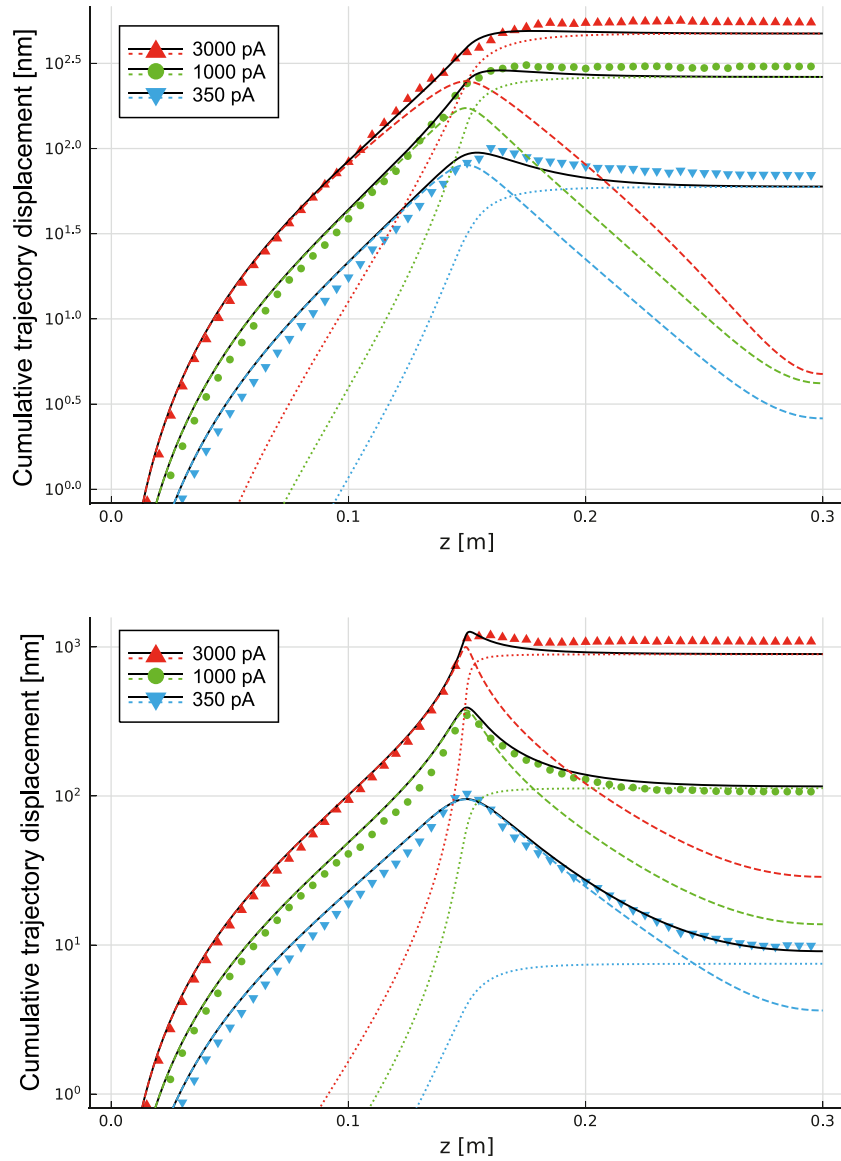


**Fig. 4.** Comparison of the new model for the slice method with a Monte Carlo simulation. The trajectory displacement is plotted as it accumulates across a multi-beam segment with a lens in the common cross-over for various beamlet currents. Top shows a typical multi-beam segment with wide common cross-over. Bottom shows the same situation with a ten-times narrower common cross-over (a hundred times larger angular current density). Solid lines represent the total trajectory displacement given by Eq. (5) with  $\gamma = 3/2$ , dashed lines correspond to the  $a$  component and dotted lines to the  $b$  component in Eq. (4), markers show the results of the Monte Carlo simulation. The low current corresponds to pencil-beam regime, the high current to Holtzmark regime and the middle current to an intermediate regime. We can see that in all cases the calculation agrees very well with the Monte Carlo simulation. We also see that in case of a narrow cross-over (bottom part with low current), the  $b$  component is smaller and the compensation of the  $a$  component is visible.

$$-F\left(\frac{-b/2 + i \cdot (a+b)}{R}\right)\Bigg\} = A - (A - B)S_2(R). \quad (8)$$

Although these expressions look complicated, their interpretation is rather simple. The maximum intensity corresponds to the situation where the spot center is in the middle of the light stripe. Thus we can calculate it as a sum of the total dark stripe intensity  $B$  and the fraction of probe located on light stripes expressed as  $S_1$  times the intensity difference  $A - B$ . Similarly we can calculate the minimum where the spot is centered in the middle of the dark stripe.

We do not know the absolute values of  $A$  and  $B$ , but we can express the ratio of the intensities  $I_1/I_2$  depending on the ratio  $A/B$  which was determined from higher resolution images to be equal to  $3.1 \pm 0.2$ :

$$\frac{I_1}{I_2} = \frac{1 + (A/B - 1)S_1(R)}{A/B - (A/B - 1)S_2(R)}. \quad (9)$$

With  $F$  known, this is a monotonous function of  $R$  which can be numerically inverted to calculate the  $E_{25,75}$  and subsequently the  $FW_{50}$

spot size. The accuracy of this measurement is in our case better than 15 nm. However, in some cases the deviation of the experimental data from the theory is larger due to random or systemic errors in acquiring the data.

#### 5.1.1. Probe distribution function

The formula for the maximum and the minimum intensity depends on the scaled linear cumulative distribution function  $F$ . This function is in general given by several combined effects:

- **The image of the virtual source.** We assume it has a gaussian distribution. Its size does not depend much on the beamlet current [6].
- **The aberrations of the optical system.** They are negligible compared to the virtual source size because the optical system is not demagnifying the virtual source.

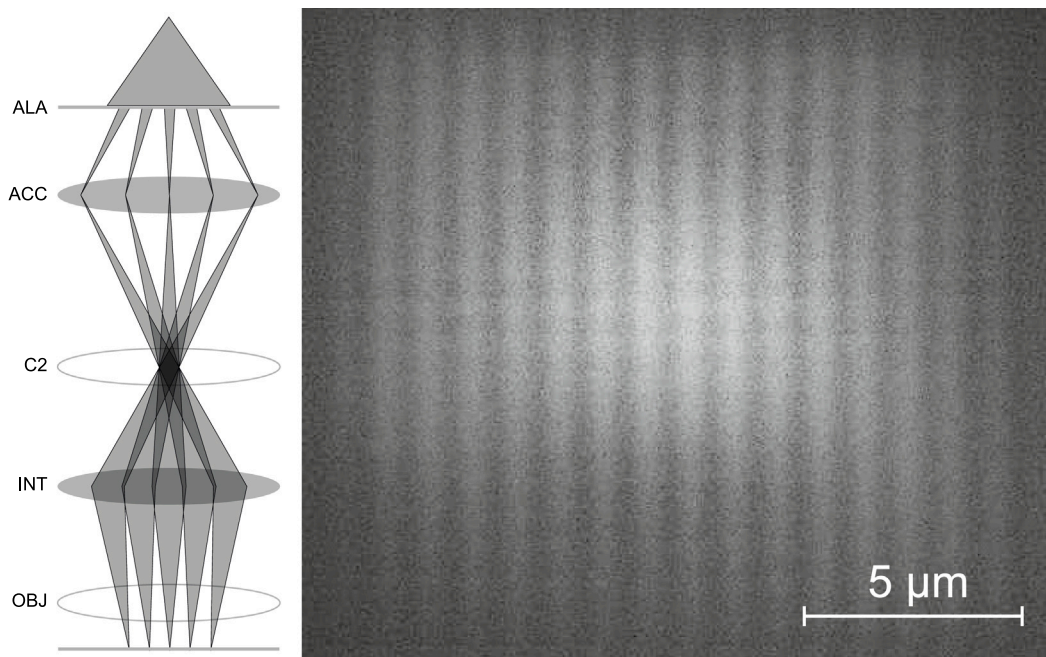


Fig. 5. Left: Schematic drawing of the system with intermediate lens used as a final lens. Right: Typical image of the sample created with one of the central beamlets for beam energy 10 keV.

- **The diffraction.** This effect is completely negligible in our system.
- **The defocus and astigmatism.** Because we use a striped sample, we can actually achieve optimal resolution even with a slight defocus or astigmatism if we use the stigmator to make a line focus with the line parallel to the stripes.
- **The trajectory displacement.** We assume the trajectory displacement has an isotropic Holtzmark distribution.

The actual distribution function is a composition of all these effects. However, we can neglect the aberrations and the diffraction. Moreover, assuming perfect line focus aligned with the sample, the spot shape is equivalent to a convolution of the stigmatic probe shape with a line segment parallel to the stripes. Because we integrate the direction parallel to the stripes out, any astigmatism is integrated out of the scaled linear cumulative distribution function.

We can determine the actual linear cumulative distribution function by taking an image of a sharp edge with a pixel resolution much larger than the probe size. The experiment verifies that the distribution function is a mix between Gaussian and Holtzmark distributions. The Gaussian contribution is larger than the Holtzmark and so for simplicity we have chosen to use a power sum rule with  $\gamma = 2$ .

## 5.2. Results and discussion

We have measured the dependence of the trajectory displacement on common cross-over position and beamlet current. The common cross-over position can be altered by changing the strength of the accelerator lens in the multi-beam source. The beamlet current was changed by manipulating the source filament temperature (changing the filament current).

In order to calculate the spot size, we need to know the position and size of the common cross-over and also the base spot size without the effect of trajectory displacement. Due to multiple unknown misalignments in the system, the position and size of the common cross-over and the spot size without Coulomb interactions are different from the theoretical values and were instead fitted to the experimental data.

Comparison of the slice method with the experimental results is shown in Fig. 6.

We see that the experimental values fit the theoretical prediction very well. Especially scaling of the trajectory displacement with respect to the beamlet current is completely in agreement with the theory, but also the dependence on the position of common cross-over seems to fit theoretical values well.

From the results we can see that the non-compensatable part of the trajectory displacement is dominant when the common cross-over is located inside the final lens. This is not surprising, because in our case the final lens is roughly in the middle of the column and thus the compensatable part vanishes in that case. We can also see that in general neither of the two contributions is negligible and both contributions have to be taken into account.

## 6. Conclusions

We started this article with a general knowledge of trajectory displacement in particle beams. We have discovered through Monte Carlo simulations that the traditional approach does not accurately describe the trajectory displacement in a multi-beam system. A detailed study of the processes causing trajectory displacement in a multi-beam system lead us to the two-component approximation.

The contribution from the vicinity of the common cross-over is in fact uncorrelated with the contributions from other parts of the trajectory, and thus the trajectory displacement can be viewed as a composition of two independent components. Furthermore, we have shown that with a suitable choice of trajectories (i.e. position of the beamlet cross-overs and common cross-overs) the component originating from outside of the common cross-over regions can be completely compensated. Unfortunately, the second contribution is always positive and therefore cannot be compensated.

The last part of the article was devoted to the experimental verification of such behavior on a multi-beam SEM with 196 beams. We were able to successfully measure the dependence of the final spot size on the beamlet current and on the shape of the optical path of the multi-beam (position of the common cross-over). The experimental results fit the predicted theoretical behavior very well and confirm that the theory can be used to describe the trajectory displacement even outside the idealized models used in Monte Carlo simulations.

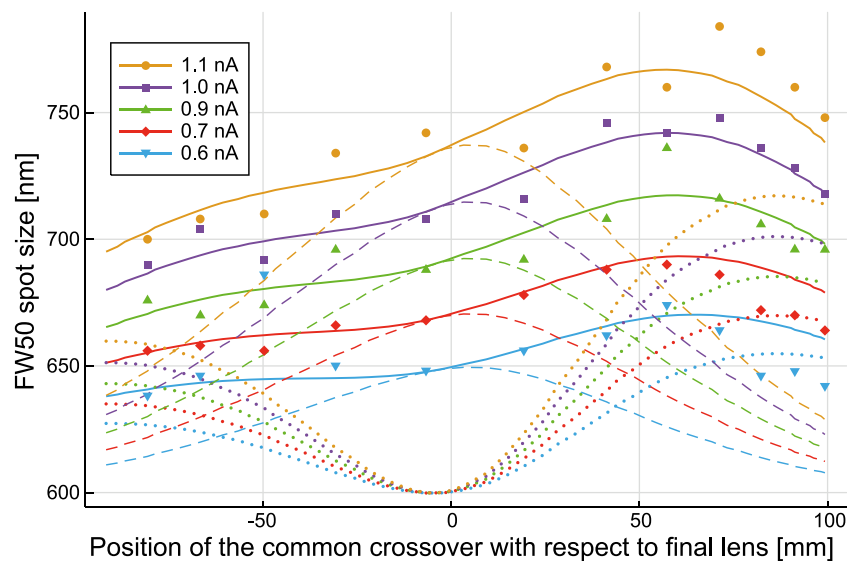


Fig. 6.  $FW_{50}$  spot size as a function of common crossover position with respect to the final lens for various beamlet currents. Markers show the experimental values, the solid line is the total calculated spot size including both contributions and a fitted intrinsic spot size. Dotted line shows results with only the compensatable  $\bar{a}$  component contribution and dashed with only the uncompensatable  $\bar{b}$  component contribution to the trajectory displacement. The accuracy of the method is below 15 nm.

We believe our work provides a valuable tool for characterization of multi-beam systems, especially for determination of resolution in probe-forming multi-beam systems such as the multi-beam SEM. It is, however, not a closed chapter as many questions remain unanswered. For example, it is not clear how to properly combine the trajectory displacement with other contributions to the final spot size such as the geometrical spot size and aberrations. Another possible path for further development is a description of trajectory displacement in case of non-ideal beam path. That includes for example enlargement of the common cross-over due to aberrations of the lens near the first beamlet crossover plane and misalignments which can potentially influence the total trajectory displacement.

To conclude, there is still a lot of room for improvement even in such a limited scope as trajectory displacement in a multi-beam SEM. Nevertheless, we have greatly improved the way trajectory displacement in these systems can be calculated and we have faith that our results will help push the field of multi-beam electron microscopy forward.

## Acknowledgments

The authors acknowledge the early involvement of Erik Kieft, Ali Mohammadi Gheidari, Bohuš Sedřa and Bas van der Geer in the Monte Carlo simulation of trajectory displacement in multi-beam systems. Jan Stopka would like to thank Tomáš Radlička of Institute of Scientific Instruments of the CAS for his helpful remarks and ThermoFisher Scientific for supporting his placement at TU Delft, where the experimental part was conducted. He would also like to thank his wife Adřela Stopka for the enormous help with creating figures for this article.

The research was supported by the TA CR, Czech Republic (TE01020118), the MEYS CR (LO1212), its infrastructure by the MEYS CR, Czech Republic and the EC, Czech Republic (CZ.1.05/2.1.0 0/01.0 017) and by the CAS, Czech Republic (RVO:68081731).

## References

- [1] G.H. Jansen, Trajectory displacement effect in particle projection lithography systems, *J. Appl. Phys.* 84 (8) (1998-10-15) 4549–4567, <http://dx.doi.org/10.1063/1.368681>, URL <http://aip.scitation.org/doi/10.1063/1.368681>.
- [2] J.E. Barth, P. Kruit, Addition of different contributions to the charged particle probe size, *Optik* 101 (1996) 101–109, URL <https://ci.nii.ac.jp/naid/80009062810/en/>.
- [3] T.R. Groves, *Charged Particle Optics Theory*, first ed., CRC Press, Boca Raton, 2015.
- [4] G.H. Jansen, *Coulomb Interactions in Particle Beams*, Academic Press, Boston, 1990.
- [5] P. Kruit, G.H. Jansen, Space charge and statistical Coulomb effects, in: J. Orloff (Ed.), *Handbook of Charged Particle Optics*, second ed., CRC Press, Boca Raton, 2009, pp. 341–389.
- [6] M.S. Bronsgeest, *Physics of Schottky Electron Sources*, Delft University of Technology, Delft, 2009.
- [7] Y. Zhang, *A 100-Electron-Beam Source from a High Brightness Schottky Emitter for Fast Patterning Applications*, Delft University of Technology, Delft, 2008.
- [8] Y. Zhang, P. Kruit, Design of a high brightness multi-electron-beam source, *Phys. Proc.* 1 (1) (2008) 553–563, <http://dx.doi.org/10.1116/1.588661>, URL <https://linkinghub.elsevier.com/retrieve/pii/S187538920800148X>.
- [9] A. Mohammadi-Gheidari, C.W. Hagen, P. Kruit, Multibeam scanning electron microscope, *J. Vac. Sci. Technol. B* 28 (6) (2010) C6G5–C6G10, <http://dx.doi.org/10.1116/1.3498749>, URL <http://avs.scitation.org/doi/10.1116/1.3498749>.
- [10] A. Mohammadi-Gheidari, P. Kruit, Electron optics of multi-beam scanning electron microscope, *Nucl. Instrum. Methods A* 645 (1) (2011) 60–67, <http://dx.doi.org/10.1016/j.nima.2010.12.090>, URL <https://linkinghub.elsevier.com/retrieve/pii/S0168900210028706>.
- [11] A. Mohammadi-Gheidari, *196 Beams in a Scanning Electron Microscope*, Delft University of Technology, Delft, 2013.
- [12] Y. Ren, P. Kruit, Transmission electron imaging in the delft multibeam scanning electron microscope 1, *J. Vac. Sci. Technol. B* 34 (6) (2016) <http://dx.doi.org/10.1116/1.4966216>, URL <http://avs.scitation.org/doi/10.1116/1.4966216>.
- [13] Y. Ren, *Imaging Systems in the Delft Multi-Beam Scanning Electron Microscope 1*, Delft University of Technology, Delft, 2017.
- [14] J. Stopka, P. Kruit, Statistical Coulomb interactions in multi-beam SEM, *Internat. J. Modern Phys. A* 34 (36) (2019) 1942021, <http://dx.doi.org/10.1142/S0217751X19420211>.
- [15] J. Stopka, Analytical formulae for trajectory displacement in electron beam and generalized slice method, *Ultramicroscopy* 217 (2020) 113050, <http://dx.doi.org/10.1016/j.ultramic.2020.113050>, URL <http://www.sciencedirect.com/science/article/pii/S0304399120302011>.
- [16] Pulsar Physics, General Particle Tracer, <http://www.pulsar.nl/gpt>.
- [17] W. Zuidema, Y. Ren, J. Hoogenboom, C. Hagen, P. Kruit, Transmission imaging of biological tissue with the delft multi-beam SEM, in: *European Microscopy Congress 2016: Proceedings*, American Cancer Society, 2016, pp. 394–395, <http://dx.doi.org/10.1002/9783527808465.EMC2016.5737>, arXiv:<https://onlinelibrary.wiley.com/doi/pdf/10.1002/9783527808465.EMC2016.5737>, URL <https://onlinelibrary.wiley.com/doi/abs/10.1002/9783527808465.EMC2016.5737>.